Enhanced Investigation of Buoyant Flow Dynamics: Thermo-Solutal Transport Alterations Induced by Nanoparticles on an Impulsively Initiated Vertical Plate

[a,b]*Nirmala.M,*[a*]*E. Geetha,*[c]*S.Sarala*

[a]*Department of Mathematics, Sri Chandrasekharendra Saraswathi Viswa Maha Vidyalaya, Enathur, Kanchipuram- 631561, India,*
[b]*Department of Mathematics, Kumararani Meena Muthiah College of Arts and Science College, Adyar, Chennai-600020, India,*
[c]*Department of Mathematics, Paavai Engineering College (Autonomous), Pachal, Namakkal- 637018, India,*

Abstract

The present investigation explores the composition of nanofluids, comprising solid nanoparticles dispersed in a conventional base fluid, emphasizing their potential to enhance thermal transport characteristics. The study examines the thermal and concentration transport behavior of a nanofluid over a vertically positioned plate subjected to an impulsive initiation. In this analysis, copper nanoparticles are considered within a water-based nanofluid. The basic dimensional formulations are transformed with their dimensionless counterparts to facilitate analytical evaluation. The flow equations, incorporating impulsive motion, and initial conditions with final constraints, have been systematically determined by applying the Laplace transform method. Graphical representations of several flow parameters are provided, such as temperature, velocity, and concentration profiles. Furthermore, a thorough analysis is conducted of the impact of important dimensionless parameters such as the Prandtl number, Schmidt number, thermal Grashof number, and mass Grashof number. The Nusselt and Sherwood numbers are computed, and the resulting fluctuations are presented in both tabular and graphical formats to provide a comprehensive insight into the thermofluidic behavior of the system.

Keywords: Heat transfer and Mass transfer, Copper Oxide Nanofluid, impulsive motion.

1. INTRODUCTION

The investigation of thermal and solutal transport in nanofluids has attracted significant research attention because of its crucial importance in various engineering fields, such as efficient thermal management, energy conversion systems, and cutting-edge manufacturing technologies. This problem serves as a crucial model for understanding numerous real-world thermal systems and has been extensively analyzed using both numerical and analytical methodologies. Researchers continue to explore the intricate coupling between heat and mass transport mechanisms in such flows, aiming to enhance the efficiency and effectiveness of thermal management strategies.

Magnetohydrodynamic (MHD) flows have received significant attention, particularly in scenarios involving impulsive motion, because of their wide-ranging applications in astrophysical engineering. Research on electrically conducting, viscous, and incompressible fluids subjected to external magnetic fields is crucial for optimizing thermal and mass transport in advanced technological systems. A fundamental problem in this field is the MHD Stokes flow, which examines transient flow characteristics over a vertically oriented infinite plate that is impulsively activated. Understanding such flows proves essential for examining intricate interactions between magnetic forces and fluid dynamics, offering critical insights into the stability and efficiency of MHD-driven thermal management systems.

Thermal and solutal transport studies make significant contributions to a wide range of engineering applications, including polymer processing, energy recovery, enhanced oil recovery, and environmental pollution control. Moreover, such investigations are highly relevant in geophysical and astrophysical phenomena, particle accelerator technologies, and metallurgical processes. Numerous theoretical studies have contributed to a deeper understanding of the transient behavior of MHD flows under varying thermal and rotational conditions, advancing the development of high-efficiency fluid transport and thermal regulation systems.

To achieve a deeper understanding of these transport phenomena, various computational and mathematical techniques have been employed. Muthucumaraswamy et al. [1] employed a numerical discretization approach to examine transient characteristics of thermal and solutal transport, providing a robust numerical framework for analyzing dynamic thermal behavior. Ramachandra Prasad et al. [2] presented a comprehensive investigation of unsteady magnetohydrodynamic (MHD) flow induced by a spontaneously initiated perpendicular plate, incorporating its influence on radiation heat. Transfer of heat through radiation inside the optically thin regime was modeled using the Rosseland approximation. To solve the nonlinear governing equations numerically, the Crank–Nicolson finite difference approach was used. Surendra Kumar and Rajput [3] probed MHD flow past an instantly initiated straight surface along varying temperatures, considering rotational and radiative effects. Their analytical solutions, obtained via the Laplace transform technique, revealed notable variations in heat transport characteristics. Similarly, Marneni

Narahari and M. Yunus Nayan [4] examined transient convective flow next to an infinite vertical surface that has been exposed to Newtonian temperature, accounting for both radiative and diffusive effects. Closed-form solutions for momentum, thermal, and fields of emphasis were derived employing the Laplace transform method, offering significant insights into unsteady thermal and mass transport phenomena.

Mehdi Rasidi et al. [5] applied the homotopy analysis method to study steady MHD move over a permeable material, including thermal radiation and non-uniform magnetism. These contributions have collectively enhanced the accuracy of computational tools in simulating complex transport phenomena. Progress in numerical techniques has led to increasingly precise modeling of nonlinear behavior in MHD and nanofluid systems. Nageeb A.H. Haroun et al. [6] utilized the spectral relaxation technique to solve a coupled set of differential equations governing the thermal and energy transport of a nanofluid flow over an instantly stretched plate. Their model considered chemical reactions, Brownian motion, and magnetohydrodynamic effects. Recent studies have also focused on how nanoparticles improve thermal transport efficiency. Loganathan et al. [7] studied nanofluid convection with internal thermal and nanoparticle impacts. Mahanthesh et al. [8] analyzed coupled thermal–energy transport with radiation, magnetism, and chemical reactions. Prasad et al. [9] modeled radiative convection with unsteady fluxes using finite differences.

Waqas Ali Azhar et al. [10] studied free convection in fractional nanofluids over a moving plate with constant heat flux, deriving exact solutions via modified Bessel functions. The findings are vital for applications in food processing, rotating machinery, and thermal systems. Abbas & Magdy [11] evaluated the thermo-physical enhancement in convective nanofluid flows over a rotating plate by viscous dissipation, The model incorporated Joule heating, Brownian motion, and thermophoretic diffusion under intense magnetic and Hall current effects, employing Cu, Al_2O_3, and TiO_2 nanoparticles of diverse morphologies-spherical, cylindrical, and brick-shaped—suspended in water. A semi-analytical solution was obtained using the homotopy perturbation method. Their findings emphasized that the shape of nanoparticles significantly affects flow characteristics, with cylindrical particles exhibiting superior thermal performance. Uwanta et al. [12] analyzed radiative effects on heat and mass transfer in Newtonian fluids along a vertical plate, revealing thermal and concentration boundary layer behavior. Rajesh et al. [13] explored MHD-free convection over an exponentially accelerated plate with radiation and variable temperature, offering insights into boundary dynamics. Anil Kumar et al. [14] investigated radiation impacts on MHD nanofluid flow past a quickly initiated surface, focusing on nanoparticle concentration and magnetic strength. Their results highlighted the role of radiative effects in improving heat transfer rates in nanofluid-based applications.

Chandrakala and Narayana Bhaskar [15] conducted an analytical investigation of MHD spread across an infinite vertical plate that started spontaneously with energy diffusion, accounting for thermal radiation. Their research yielded precise answers for the profiles of temperature, concentration, and velocity. In a radiatively influenced boundary layer flow past a sliding vertical plate within a free stream, Patil [16] examined mixed convection with thermophoretic effects. Their analytical model considered buoyancy and thermophoretic forces, with implications for heat exchanger and aerosol transport technologies. Visalakshi and Vasanthabhava M [17] examined transient heat and energy transport along a parabolically accelerated perpendicular surface subjected to a steady flow of heat. They derived exact solutions to assess heat and mass diffusion on flow rate and temperature variations. Absana Tarammim et al. [18] numerically investigated an unstable two-dimensional MHD convection that moves freely across a plate that is vertical, incorporating buoyancy forces and magnetic field effects. Their simulations detailed the temporal evolution of temperature, velocity, and concentration distributions. Kamalesh Kumar Pandit et al. [19] explored unsteady radiation-filled MHD flow over an abruptly initiated perpendicular surface, formulating dimensionless equations to capture variations in temperature and velocity under different parameter settings. Their results provide practical insights into industrial heat and fluid flow systems.

Khan and Solanki [20] conducted a study on the free convection flow that is unstable across an endless perpendicular plate, incorporating the possessions of thermal radiation and mass transfer. By employing analytical methods, they addressed the governing equations and explored the impacts of radiative thermal transmission in addition to species dispersion on the movement characteristics.

2. MATHEMATICAL ANALYSIS

Consider the transient flow of a viscous, incompressible nanofluid over an infinitely long vertical plate impulsively set in motion. The flow progresses along the x′-axis, parallel to the plate, with the y′-axis extending normally to its surface, as depicted in Fig. 1.

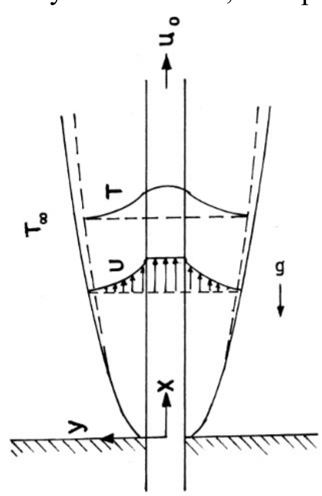

Fig 1. Geometrical representation

The ambient temperature surrounding the plate is denoted by T_∞ Under steady-state conditions, the vertical plate is maintained in a stationary position. The adjacent fluid is with consistent temperature and absorption at the time. $t^{'} \leq 0$. At time $t^{'} > 0$, an impulsive motion is liable on the plate in the upright way. Here the velocity is taken as constant, and it is denoted as u_0.

In the present investigation, water serves as the base fluid for the nanofluid system, with copper (Cu) and copper oxide (CuO) employed as the suspended nanoparticles. The nanoparticle-base fluid mixture is assumed to be in thermal equilibrium, ensuring uniform temperature distribution throughout the fluid medium. Table 1 outlines the thermophysical properties of the nanofluids, including density, specific heat, thermal conductivity, and dynamic viscosity.

The governing equations are derived under the classical Boussinesq approximation, wherein density variations are considered solely within the buoyancy term, while the fluid is otherwise treated as incompressible.

Table1.Thermo physical values of copper and water nanoparticles

Physical Properties	Water/Base fluid	Copper
$\rho(kg/m^3)$	997.1	8933
$C_\rho(J/kgK)$	4179	385
$K(W/mK)$	0.613	401
$\beta\times10^5(K^{-1})$	21	1.67
$\beta^*\times10^6(m^2/\mathrm{h})$	298.2	3.05
ϕ	0.0	0.05
$\sigma(S/m)$	5.5×10^{-6}	$59.6X10^6$

The governing equations are formulated under the standard Boussinesq approximation.

$$\rho_{nf}\frac{\partial u^{'}}{\partial t^{'}}=g(\rho\beta)_{nf}(T^{'}-T_\infty^{'})+g(\rho\beta^*)_{nf}(C^{'}-C_\infty^{'})+\mu_{nf}\frac{\partial^2u^{'}}{\partial y^{'2}} \tag{1}$$

$$\left(\rho C_\rho\right)_{nf}\frac{\partial T^{'}}{\partial t^{'}}=k_{nf}\frac{\partial^2T^{'}}{\partial y^{'2}} \tag{2}$$

$$\frac{\partial C^{'}}{\partial t^{'}}=D_{nf}\frac{\partial^2C^{'}}{\partial y^{'2}} \tag{3}$$

Here the velocity component, 'u', is taken in the horizontal way that is along$xaxis$. The values of these nanofluid coefficients are:

$$\mu_{nf}=\frac{\mu_f}{(1-\phi)^{2.5}}, \tag{4}$$

$$\rho_{nf}=(1-\phi)\rho_f+\phi\rho_s \tag{5}$$

$$\left(\rho C_\rho\right)_{nf}=(1-\phi)\left(\rho C_\rho\right)_f+\phi\left(\rho C_\rho\right)_s \tag{6}$$

The terms given in equation (1) are confined to spherical nanoparticles. The other shapes of nanoparticles are not taken into consideration.

$$k_{nf}=k_f\left[\frac{k_s+2k_f-2\phi\left(k_f-k_s\right)}{k_s+2k_f+\phi\left(k_f-k_s\right)}\right] \tag{7}$$

In equations (1)–(7), *nf*, *f*, and *s* denote the properties of the nanofluid, base fluid, and nanoparticles, respectively, with the following initial and boundary conditions.

$$t' \leq 0; \quad u' = 0, \quad T' = T'_{\infty}, \quad C' = C'_{\infty}, \quad \forall y' \leq 0$$
$$t' > 0; \quad u' = u_0, \quad \frac{\partial T'}{\partial y'} = -\frac{q}{K}, \quad \frac{\partial C'}{\partial y'} = -\frac{j''}{D} at \quad y' = 0$$
$$t' > 0; \quad u' \to 0, \quad T' \to T'_{\infty}, \quad C' \to C'_{\infty}, \quad as \; y' \to \infty$$

Using nondimensional quantities,

$$U = \frac{u'}{u_0}, \quad t = \frac{t' u_0^2}{v_f}, \quad Y = \frac{y' u_0}{v_f}$$

$$\theta = \frac{T' - T'_{\infty}}{\left(\frac{q v_f}{K_f u_0}\right)}, \quad C = \frac{C' - C'_{\infty}}{\left(\frac{j'' v_f}{D_f u_0}\right)}$$

$$G_r = \frac{g\beta v_f\left(\frac{q v_f}{K_f u_0}\right)}{u_0^3}, P_r = \frac{\mu C_p}{k_f}$$

$$G_c = \frac{g\beta^* v_f\left(\frac{j'' v_f}{D_f u_0}\right)}{u_0^3}, \quad S_c = \frac{v_f}{D_f}$$

By using equations from Eq, (4) to Eq. (7), equations from Eq. (1) to Eq. (3) restrained to

$$L_1 \frac{\partial U}{\partial t} = L_3 \frac{\partial^2 U}{\partial Y^2} + L_2 G_r \theta + L_4 G_c C \tag{8}$$

$$L_5 \frac{\partial \theta}{\partial t} = L_6 \frac{1}{P_r} \frac{\partial^2 \theta}{\partial Y^2} \tag{9}$$

$$\frac{\partial C}{\partial t} = \frac{1}{S_c} \frac{\partial^2 C}{\partial Y^2} \tag{10}$$

Where

$$L_1 = (1-\phi) + \phi\left(\frac{\rho_s}{\rho_f}\right)$$

$$L_2 = (1-\phi) + \phi\left(\frac{(\rho\beta)_s}{(\rho\beta)_f}\right)$$

$$L_3 = \frac{1}{(1-\phi)^{2.5}}$$

$$L_4 = (1-\phi) + \phi\left(\frac{(\rho\beta^*)_s}{(\rho\beta^*)_f}\right)$$

$$L_5 = (1-\phi) + \phi\left(\frac{\left(\rho C_\rho\right)_s}{\left(\rho C_\rho\right)_f}\right)$$

$$L_6 = \left[\frac{k_s + 2k_f - 2\phi\left(k_f - k_s\right)}{k_s + 2k_f + \phi\left(k_f - k_s\right)}\right]$$

The equivalent initial conditions and the boundary conditions are

$$\begin{array}{lllll} t \le 0; & U = 0, & \theta = 0, & C = 0, & \forall y \le 0 \\ t > 0; & U = 1, & \frac{\partial \theta}{\partial y} = -1, & \frac{\partial C}{\partial y} = -1 & at y = 0 \\ t > 0; & U \to 0, & \theta \to 0, & C \to 0 & as y \to \infty \end{array} \tag{11}$$

3. SOLUTION PROCEDURE

Exponential and complementary error function terms are used to portray the solutions.

$$erfc(x) = 1 - \mathrm{erf}(x) \tag{12}$$

The equations depict between error and its complementary error relation. The governing equations with dimensionless quantities Eq. (8), Eq. (9), and Eq. (10) subject to the conditions in Eq. (11), are solved using the Laplace transform, and the corresponding solutions are presented below.

$$\theta = \frac{2\sqrt{t}}{\sqrt{a}}\left(\frac{1}{\sqrt{\pi}} exp(-a\eta^2) - \sqrt{a}\eta . erfc\left(\sqrt{a}\eta\right)\right) \tag{13}$$

Case (i) For $S_c \neq 1$

$$U = erfc\left(\sqrt{g}\eta\right) + \frac{bt^{\frac{3}{2}}}{3\sqrt{a}}\left[\frac{4}{\sqrt{\pi}}(1 + g\eta^2)exp(-g\eta^2) - \frac{4}{\sqrt{\pi}}(1 + a\eta^2)exp(-a\eta^2) + \eta\sqrt{a}(6 + 4a\eta^2)erfc\left(\sqrt{a}\eta\right) - \eta\sqrt{g}(6 + 4g\eta^2)erfc\left(\sqrt{g}\eta\right)\right] + \frac{dt^{\frac{3}{2}}}{3\sqrt{S_c}}\left[\frac{4}{\sqrt{\pi}}(1 + g\eta^2)exp(-g\eta^2) - \frac{4}{\sqrt{\pi}}(1 + S_c\eta^2)exp(-S_c\eta^2) + \eta\sqrt{S_c}(6 + 4S_c\eta^2)erfc\left(\sqrt{S_c}\eta\right) - \eta\sqrt{g}(6 + 4g\eta^2)erfc\left(\sqrt{g}\eta\right)\right] \tag{14}$$

$$C = \frac{2\sqrt{t}}{\sqrt{S_c}}\left(\frac{1}{\sqrt{\pi}} exp(-S_c\eta^2) - \sqrt{S_c}\eta erfc\left(\sqrt{S_c}\eta\right)\right) \tag{15}$$

Where $a = \frac{L_5 P_r}{L_6}$, $b = \frac{L_2 G_r}{L_3 a - L_1}$, $d = \frac{L_4 G_c}{(S_c L_3 - L_1)}$, $g = \frac{L_1}{L_3}$

Case (i) For $S_c = 1$

$$C = 2\sqrt{t}\left(\frac{1}{\sqrt{\pi}} exp(-\eta^2) - \eta erfc(\eta)\right) \tag{16}$$

$$U = erfc\left(\sqrt{g}\eta\right) + \frac{bt^{\frac{3}{2}}}{3\sqrt{a}}\left[\begin{array}{l}\frac{4}{\sqrt{\pi}}(1 + g\eta^2)exp(-g\eta^2) - \frac{4}{\sqrt{\pi}}(1 + a\eta^2)exp(-a\eta^2) + \\ \eta\sqrt{a}(6 + 4a\eta^2)erfc\left(\sqrt{a}\eta\right) - \eta(6 + 4g\eta^2)erfc\left(\sqrt{g}\eta\right)\end{array}\right] \tag{17}$$

4. CONSEQUENCES AND DISCUSSION

Velocity, temperature, and concentration profiles are analytically determined through the application of the Laplace transform technique. In this analysis, a copper–water-based nanofluid is considered, with copper nanoparticles dispersed in water serving as the base fluid.

4.1 CONSEQUENCE VELOCITY PROFILE FACTORS:

Figure 2 illustrates the velocity distribution of a copper–water nanofluid about the similarity variable η for different Schmidt number (Sc) values, with all other parameters, maintained constantThe velocity profile is seen to reduce progressively as Sc increases, as illustrated in Fig.2.This inverse trend can be attributed to the physical interpretation of the Schmidt number, which characterizes the relationship between kinematic viscosity and mass diffusivity. Higher Sc values imply lower mass diffusivity, thereby intensifying resistance to momentum transport and leading to a reduction in fluid velocity. Moreover, at lower Schmidt numbers, a thicker boundary layer is observed near the plate, indicating stronger convective motion and enhanced momentum diffusion in the region adjacent to the surface.

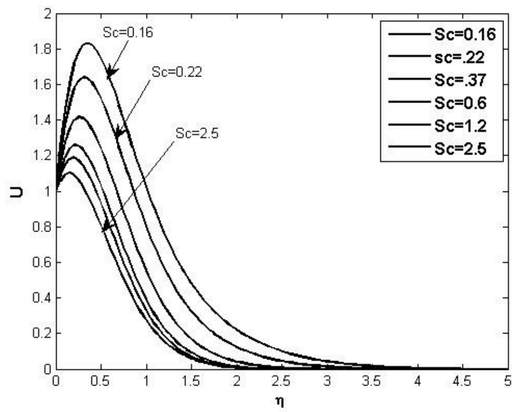

Fig 2. Flow rate with changing 'Sc' values

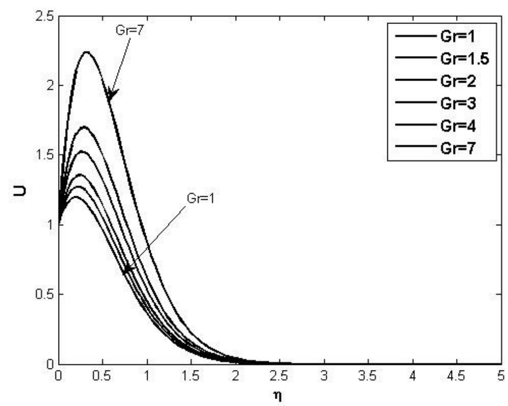

Fig3. Flow rate with changing 'Gr' values

The impact of the thermal Grashof number (Gr) on flow dynamics is presented in Fig.3.The results indicate that as Gr increases, the flow rate of the fluid increases in response, indicating a pronounced effect of buoyancy-induced thermal forces on the flow dynamics. This phenomenon arises from buoyancy forces generated by temperature gradients, which aid fluid motion near the oscillating plate An influence of elasticity becomes more pronounced as Gr increases, reinforcing the convective motion in the nanofluid. In this analysis, the Schmidt number is considered to be Sc=0.6

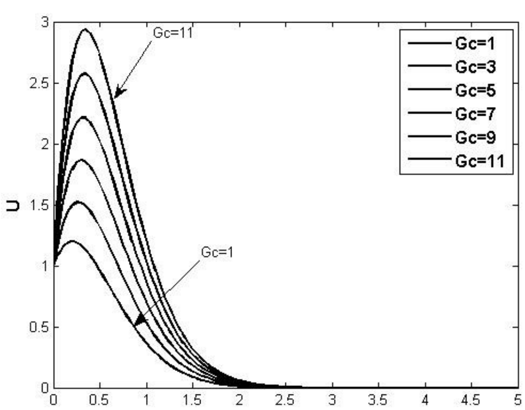

Fig 4. Flow rate with changing 'Gc' values

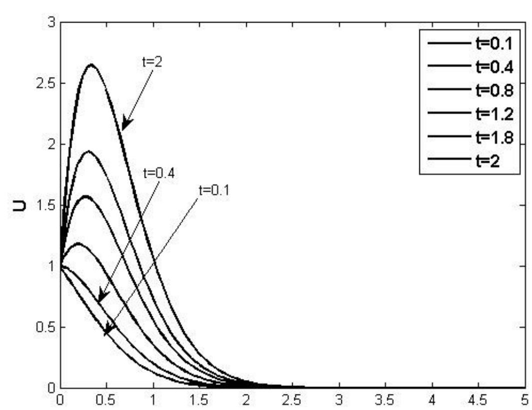

Fig5.Flow rate with changing 't' values

Figure 4 demonstrates how the mass Grashof number (Gc) affects flow velocity. Gc quantifies the balance between buoyancy and viscous forces arising from mass concentration variations. As Gc increases, the buoyancy effect intensifies, promoting natural convection. This augmentation results in an increased fluid velocity, particularly within the near-wall region. A higher Gc facilitates greater momentum transfer, diminishing viscous resistance. As a result, the velocity profile becomes more distinct, improving the efficiency of mass transport.

Fig 5. demonstrates the time-dependent evolution of the velocity profile. As time progresses, velocity increases under the sustained influence of external forces like buoyancy, thermal effects, and concentration gradients. These forces gradually enhance fluid motion while diminishing viscous resistance. Consequently, velocity continues to rise until it stabilizes at a steady state or equilibrium condition.

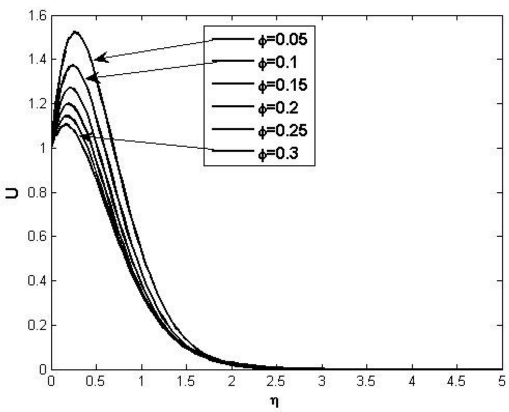

Fig 6. Flow rate with changing $'\phi'$values

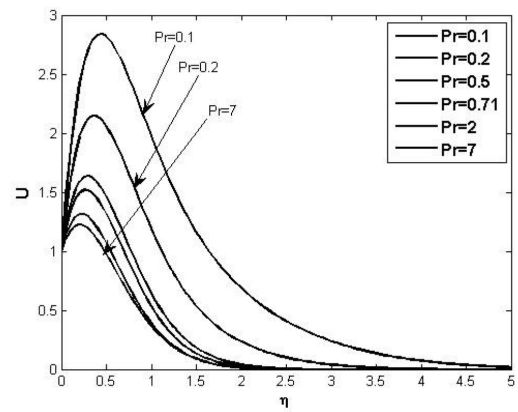

Fig 7. Flow rate with changing $'Pr'$values

Elevated solid volume fractions result in greater nanofluid viscosity, intensifying the opposition to fluid motion. The higher density enhances inertia, demanding greater force to maintain movement. A greater particle concentration disturbs fluid momentum, leading to a reduction in velocity. Increased drag and friction from particle interactions further impede fluid motion. As a result, a higher solid volume fraction causes a decline in velocity in Fig.6.As the Prandtl number (Pr) increases in Fig. 7, fluid viscosity rises, enhancing resistance to motion. The dominance of momentum diffusion over thermal diffusion reduces convective effects, slowing the fluid. Increased viscosity suppresses acceleration, leading to a lower velocity profile. Consequently, higher Pr results in greater resistance and decreased velocity.

4.2 IMPACT OF KEY PARAMETERS ON THERMAL AND CONCENTRATION PROFILES.

Figure 8 depicts how the Schmidt number (Sc) affects the concentration field**,** where a decline in concentration is observed as Sc increases while maintaining other parameters constant. This trend is ascribed to the inverse correlation between the Schmidt number (Sc) and mass diffusivity, where Sc = ν/D. Augmented Schmidt number indicate reduced molecular diffusion of solute particles, leading to a more constrained concentration boundary layer. As a result, solute transport is suppressed, and concentration levels decrease within the fluid domain. Conversely, for lower Schmidt numbers, the mass diffusivity is higher, facilitating greater dispersion and sustaining a higher concentration gradient near the oscillating plate.

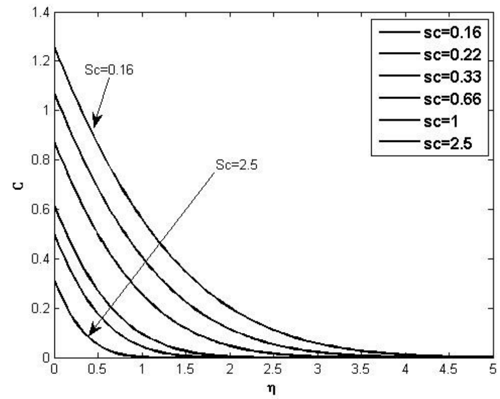

Fig 8. Concentration profile with different 'Sc'

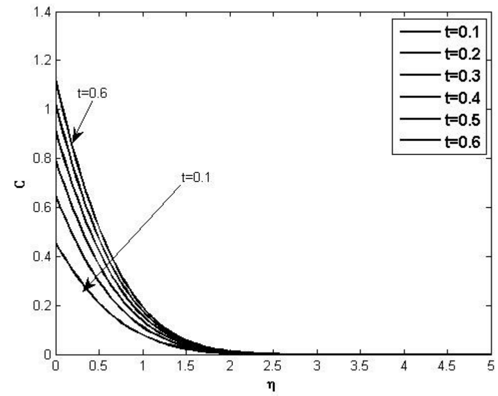

Fig 9. Concentration profile with different 't'

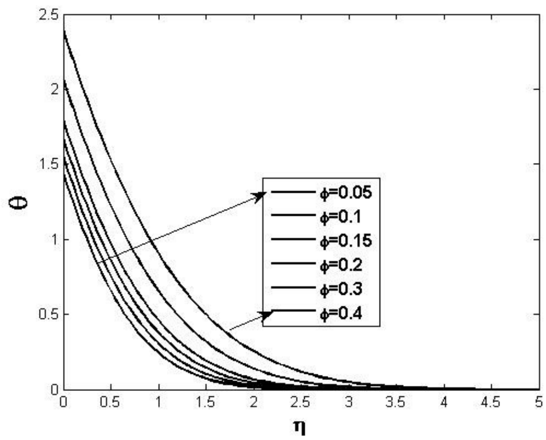

Fig 10. Temperature response for distinct 'ϕ'

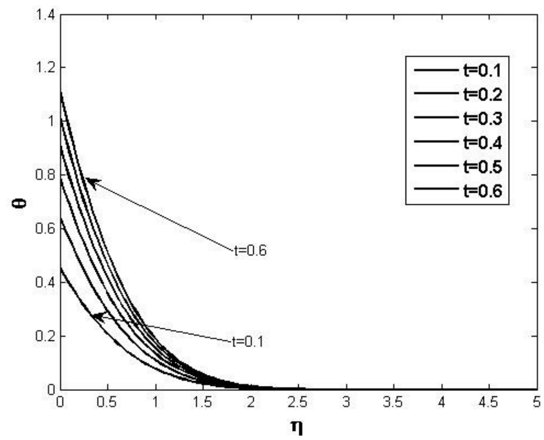

Fig.11 Temperature response for distinct 't'.

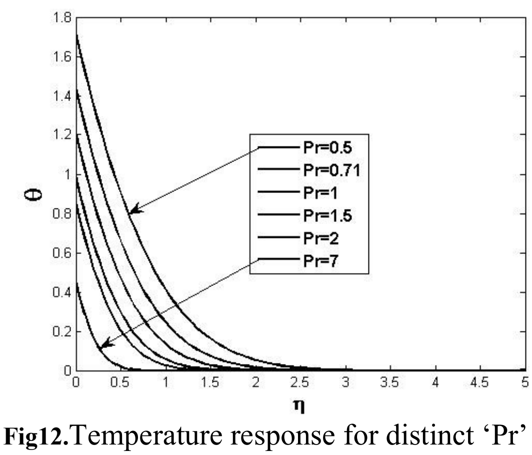

Fig12. Temperature response for distinct 'Pr'

As time increases, particles continue to diffuse and accumulate, leading to higher concentrations in Fig.9. In systems with variable concentration, regions with higher initial concentrations diffuse into lower ones, increasing overall concentration. This process continues as long as there's a concentration gradient, driving the accumulation over time. As time progresses, heat accumulates within the nanofluid, leading to a rise in temperature. Additionally, increasing the solid volume fraction enhances thermal conductivity, facilitating more efficient thermal transport. This results in greater thermal energy retention within the fluid, further elevating its temperature. Consequently, both time and solid volume fractions contribute to the observed temperature increase in Fig10 and Fig 11.

Fig. 11 demonstrates a decreasing trend with a rising Prandtl number (Pr). where $Pr = \nu/\alpha$.A higher Pr indicates lower thermal diffusivity, implying reduced heat diffusion, thereby indicating diminished thermal conductivity in the nanofluid. Consequently, higher Prvalues result in diminished thermal transport efficiency, restricting thermal diffusion and leading to a thinner thermal boundary layer. This phenomenon is evident in fluids with high Prandtl numbers, where convective thermal transport is dominant, but thermal conduction remains weak, causing a steeper temperature gradient. The findings underscore the critical role of Prin governing the thermal response of nanofluids, highlighting its importance in optimizing thermal transport mechanisms in industrial and engineering applications involving MHD nanofluid flow over oscillating plates.

4.3 ANALYSIS OF PARAMETERS OF NUSSELT NUMBER AND SHERWOOD NUMBER

The dimensionless expression for the thermal transport rate, represented by the Nusselt number, takes the following form.

$$Nu = -\left(\frac{\partial \theta}{\partial y}\right)_{y=0}$$

A Nusselt number of unity implies that heat is transferred solely by conduction, indicating a quiescent fluid. When the Nusselt number exceeds one, it signifies that convective heat transfer dominates over conduction, reflecting enhanced thermal transport due to fluid motion.

Table 2. Nusselt Number Variation with Key Parameters

Pr	t	ϕ	Nu
0.71	0.5	0.05	1.0231
2			0.6096
5			0.3855
7.1			0.3235
0.71	0.1	0.05	0.4575
	0.5		1.0231
	0.75		1.2530
	1		1.4468
0.71	0.5	0.05	1.0231
		0.1	1.1024
		0.15	1.1856
		0.2	1.2736

Table 2 presents the computed Nusselt number (Nu) values corresponding to various parametric settings, offering a comprehensive understanding of the thermal transport behavior within the nanofluid system. The significant trend that emerges from the Nusselt number exhibits a decreasing behavior with increasing Pr while keeping time (t) and heat

source parameter (q) fixed. This inverse relationship arises due to the fundamental definition of Pr, it represents the ratio between momentum diffusivity and thermal diffusivity. An increase in the Prandtl number implies a decline during the fluid's heat diffusion, thereby suppressing conductive heat transfer. As a result, the temperature gradient near the surface intensifies, leading to a thinner thermal layer and subsequently a lower Nusselt number, indicating diminished surface heat transfer.
Conversely, The Nusselt number exhibits a progressive increase over time, indicating that as the system evolves, the thermal boundary layer develops further, facilitating enhanced convective heat transfer. The numerical properties of ϕ, t, and Pr on thermal transport coefficients are systematically evaluated and tabulated in Table 2**,** emphasizing their role in governing the transport phenomena within the nanofluid system.

The concentration distribution is utilized to evaluate the rate of mass diffusion, which is represented using the Sherwood number as follows:

$$S\mathbf{h} = -\left(\frac{\partial C}{\partial y}\right)_{y=0}$$

Using specified boundary conditions, its numerical values have been computed and are presented in Table 3.

Table3.Parametric Influence on the Sherwood Number

t	**Sc**	**Sh**	**t**	**Sc**	**Sh**
0.1	0.1	1.1284	0.1	0.75	0.4120
0.2		1.5958		1	0.3568
0.3		1.9544		2	0.2523
0.4		2.2568			
0.5		2.5231			
1		3.5682			
0.1	0.16	0.8921	0.5	0.75	0.9213
0.2		1.2616		1	0.7979
0.3		1.5451		2	0.5642
0.4		1.7841			
0.5		1.9947			
1		2.8209			
0.1	0.3	0.6515	1	0.75	1.3029
0.2		0.9213		1	1.1284
0.3		1.1284		2	0.7979
0.4		1.3029			
0.5		1.4567			
1		2.0601			

The Sherwood number (Sh), representing the efficiency of Substance transfer, exhibits a comparable behavior concerning solutal transport processes. It is particularly associated with the characteristics of the concentration gradient region adjacent to the surface, whereas the Nusselt number is associated with the fluid layer adjacent to the heated surface. Both parameters collectively determine the efficiency of thermal and substance surface convection.

The Sherwood number is seen to decline as the Schmidt number rises, while it rises with the progression of time. An increase in the Sherwood number with time is attributed to the gradual evolution of the concentration boundary layer. Over time, molecular diffusion allows for more effective solute transport within the fluid, leading to an enhanced convective mass transfer rate. This results in an increase in Sherwood number, as more mass is transported across the boundary layer with time. These findings are crucial for optimizing mass transport performance in nanofluid-based thermal exchangers, MHD flow systems, and advanced cooling technologies.

The coefficient of surface shear is a fundamental parameter within fluid dynamics, defining the dimensionless shear stress exerted by a fluid on a solid boundary. It characterizes the resistance experienced by fluid in motion due to viscosity and plays a crucial role in studying boundary layer behavior, drag minimization, and energy dissipation across various engineering and industrial applications.

$$c_f = -\left(\frac{\partial U}{\partial y}\right)_{y=0}$$

Table 4. Parametric Influence on Skin Friction Coefficient

ϕ	t	Gr	Gc	Pr	Sc	c_f
0.05 **0.10** **0.15**	0.2	3	5	0.71	0.6	0.4206 0.6202 0.7590
0.05	**0.3** **0.6** **0.9**	5	6	0.71	0.6	-0.8507 -4.6940 -9.6709
0.05	0.4	**6** **7** **8**	9	0.71	0.6	-3.1563 -3.4541 -3.7519
0.05	0.5	5	**8** **10** **12**	0.71	0.6	-4.0854 -4.8993 -5.7133
0.05	0.6	3	5	**0.71** **3.1** **7.1**	0.6	-3.0649 -1.9653 -1.6978
0.05	0.1	4	8	0.71	**0.6** **1.2** **1.8**	0.8112 0.9264 0.9732

In Table 4, an increase in particle size and Schmidt number (Sc) results in a rise in the coefficient of surface shear due to stronger viscous effects. A larger particle size enhances the nanofluid's viscosity, amplifying shear forces along the surface. A higher Sc lowers mass diffusivity, resulting in steeper velocity gradients near the boundary. This intensifies shear stress, directly elevating c_f. Moreover, increased particle interactions and momentum resistance further heighten frictional forces. Thus, the combined influence of viscosity, diffusivity, and wall shear stress contributes to a greater skin friction coefficient. As the Prandtl number (Pr) increases, viscosity rises, enhancing shear stress at the surface and leading to a higher coefficient of surface shear. Lower thermal diffusivity causes a thinner velocity boundary layer, amplifying velocity gradients near the wall. As a result, greater viscosity and shear forces contribute to an increase in c_f.

As time progresses, the velocity profile stabilizes, reducing shear stress at the surface and lowering the coefficient of surface shear. An increasing thermal Grashof number (Gr) enhances buoyancy forces, promoting free convection and diminishing the influence of viscous effects, leading to a decline in the coefficient of surface shear. Similarly, a higher mass Grashof number (Gc) intensifies concentration-driven buoyancy forces, accelerating the fluid while reducing shear resistance at the wall. Stronger natural convection effects cause boundary layer expansion, decreasing velocity gradients near the surface. This expansion weakens the shear forces acting on the wall, further reducing c_f. Thus, as time, Gr, and Gc increase, the coefficient for surface shear decreases due to diminished shear stress.

5 CONCLUSION

This study explores the influence of thermal and solutal transport within a nanofluid system subjected to an impulsively initiated vertical plate. The selected parameters' impact on U, θ, and C is thoroughly examined. The outcomes of this research offer a valuable understanding of the thermofluid behavior of nanofluids in the context of MHD and convective thermal transport systems. The principal findings are outlined below:

(i). Velocity reduction with higher Schmidt numbers: The velocity profile exhibits a decreasing trend with increasing Schmidt number (Sc), which is attributed to the reduction in mass diffusivity, leading to a suppressed convective motion within the boundary layer.

(ii). Influence of Gr and mass Gc on flow rate: A rise in both the Gr and Gc results in an enhancement of velocity due to intensified buoyancy-driven forces.

(iii). Concentration profile dynamics: The concentration profile declines along high Sc, as higher Sc restricts mass transport. However, as time progresses, the concentration profile exhibits a growth due to sustained diffusion effects.

(iv). Temperature profile behavior: The temperature profile is inversely related to the Prandtl number (pr), indicating that higher values of pr reduce thermal diffusivity, resulting in a thinner thermal boundary layer and lower temperatures.

(v). Nusselt number trends: The Nusselt number, representing the thermal transport rate, reduces by way of a huge Prandtl number however, it rises progressively over time and nanoparticle size, highlighting the role of thermal conductivity enhancement in nanofluid systems.

(vi). Sherwood number variation: The Sherwood number, which quantifies mass transfer, rises with time for various Schmidt number values, demonstrating enhanced solute transport over extended durations.

These findings contribute to the fundamental understanding of nanofluid dynamics and offer potential implications for applications in thermal energy management, MHD boundary layer flow, and advanced cooling systems.

Acknowledgement:
I am grateful to Dr. E. Geetha, Assistant Professor, Sri ChandraSekharendraSaraswathiViswa Maha Vidyalaya, Enathur, Kanchipuram for her meticulous guidance and unconditional support in completing this paper.

NOMENCLATURE

List of symbols

C'	Species Concentration near the plate.
C'_∞	Species Concentration in the fluid far away from the plate
C	dimensionless concentration
C_p	Specific heat at constant pressure
D	mass diffusion coefficient
G	acceleration due to gravity
G_r	thermal Grashof number
G_r	mass Grashof number
j''	Mass flux per unit area at the plate
K	thermal conductivity of the fluid
Nu	Nusselt number
Pr	Prandtl number
q	heat flux per unit area at the plate
Sc	Schmidt number
t'	time
T	dimensionless time
T'	temperature of the fluid near the plate
T'_∞	temperature of the fluid far away from the plate
T'_w	the temperature of the plate
u'	velocity of the fluid in the x' - direction
u_0	velocity of the plate
u	dimensionless velocity
x'	Coordinate axis along the plate.
y'	coordinate axis normal to the plate
y	dimensionless coordinate axis normal to the plate
β	Volumetric coefficient of thermal expansion
β^*	Volumetric coefficient of expansion with concentration
µ	coefficient of viscosity
ν	kinematic viscosity
Q	density
τ'	skin-friction
τ	dimensionless skin-friction
θ	dimensionless temperature
$erfc$	complementary error function
η	similarity parameter

REFERENCES:

1. R.Muthucumaraswamy, P. Ganesan 'Flow past an impulsively started vertical plate with constant heat flux and mass transfer' Comput. Methods Appl. Mech. Engrg. 187 (2000) 79-90.

2. V. Ramachandra Prasad, N. Bhaskar Reddy, R.Muthucumaraswamy, 'Transient radiative hydromagnetic free convection flow past an impulsively started vertical plate with uniform heat and mass flux', Theoret. Appl. Mech., Vol.33, No.1, pp. 31{63, Belgrade 2006.
3. U. S. Rajput and Surendra Kumar, 'Rotation and Radiation Effects on MHD Flow Past an Impulsively Started Vertical Plate with Variable Temperature', Int. Journal of Math. Analysis, Vol. 5, 2011, no. 24, 1155 – 1163.
4. MarneniNarahari, M. YunusNayan, 'Free convection flow past an impulsively started infinite vertical plate with Newtonian heating in the presence of thermal radiation and mass diffusion' Turkish J. Eng. Env. Sci. 35 (2011), 187 – 198. © TUB¨ ˙ ITAK doi: 10.3906/muh-1101-15.
5. Mohammad Mehdi Rashidi, BehnamRostami, NavidFreidoonimehr, SaeidAbbasbandy, Free Convective heat and mass transfer for MHD fluid flow over a permeable vertical stretching sheet in the presence of the radiation and buoyancy effects, Ain Shams Engineering Journal, (2014), 5,901-912.
6. Nageeb AH Haroun, Precious Sibanda, Sabyasachi Mondal, Sandile S Motsa, and Mohammad M Rashidi, 'Heat and mass transfer of nanofluid through an impulsively vertical stretching surface using the spectral relaxation method', Haroun et al. Boundary Value Problems (2015) 2015:161 DOI 10.1186/s13661-015-0424-3.
7. P. Loganathan, P. Nirmal Chand &P. GanesanTransient natural convective flow of a nanofluid past a vertical plate in the presence of heat generation *Journal of Applied Mechanics and Technical Physics* volume 56, pages433–442(2015)
8. B.Mahanthesh, B.J.Gireesha, Rama Subba Reddy Gorla, Heat and mass transfer effects on the mixed convective flow of chemically reacting nanofluid past a moving/stationary vertical plate, Alexandria Engineering JournalVolume 55, Issue 1, March 2016, Pages 569-581
9. V.R. Prasad, N. Bhaskar Reddy, R. Muthucumaraswamy and B.Vasu, 'Finite Difference Analysis of Radiative Free Convection Flow Past an Impulsively Started Vertical Plate with Variable Heat and Mass Flux' Journal of Applied Fluid Mechanics, Vol. 4, No. 1, 59-68, 2011, ISSN 1735-3645.
10. Waqas Ali Azhar, Dumitru Vieru, Constantin Fetecau, Free convection flow of some fractional nanofluids over a moving vertical plate with uniform heat flux and heat source Physics of Fluids 29, 082001 (2017); https://doi.org/10.1063/1.4996034
11. W. Abbas and M. M. Magdy, Heat and Mass Transfer Analysis of Nanofluid Flow Based on, cu, Al_2O_3, and Tio_2 over a Moving Rotating Plate and Impact of Various Nanoparticle Shapes, Hindawi Mathematical Problems in Engineering Volume 2020, Article ID 9606382, 12 pages
12. I. J. Uwanta, A.Ahmed 'Radiation Effects on Heat and Mass Transfer over a vertical plate with Newtonian Fluid' International Journal Of Research And Technology (Ijert), ISSN 2278-0181, Vol I, Issue 8, October 2012.
13. V. Rajesh and S. Vijaya Kumar Varma, 'Radiation and Mass Transfer Effects On MHD Free Convection Flow Past An Exponentially Accelerated Vertical Plate With Variable Temperature' ARPN Journal Of Engineering And Applied Sciences, Issn 1819-6608, Vol. 4, No. 6, August 2009.
14. M. Anil Kumar, Y. Dharmendar Reddy, V. Srinivasa Rao a, B. Shankar GoudThermal radiation impact on MHD heat transfer natural convective nanofluid flow over an impulsively started vertical plate, Case Studies in Thermal EngineeringVolume 24, April 2021, 100826.

15. P. Chandrakala P. Narayana Bhaskar, ‘Radiation Effects On MHD Flow Past an Impulsively Started Infinite Vertical Plate with Mass Diffusion’ Int. Journal of Applied Mechanics and Engineering, 2014, vol.19, No.1, pp.17-26 DOI: 10.2478/ijame-2014-000.
16. P.M.Patil, ‘Effects of thermophoresis on mixed convection flow from a moving vertical plate in a parallel free stream in the presence of thermal radiation’ IOSR Journal of Mathematics (IOSR-JM) e-ISSN: 2278-5728,p-ISSN: 2319-765X, Volume 7, Issue 4 (Jul. - Aug. 2013), PP 82-92.
17. V. Visalakshi, K.VasanthabhavaM, ‘Heat And Mass Transfer Effects On Flow Past Parabolic Started Vertical Plate With Constant Heat Flux’, International Journal of Advancements in Research & Technology, Volume 3, Issue 4, April-2014, ISSN 2278-7763
18. AbsanaTarammim, Mohammad Sharif Ullah, Mohammed Jahir Uddin, ‘A Study of Two-Dimensional Unsteady MHD Free Convection Flow over a Vertical Plate’ Open Journal of Fluid Dynamics, 2020, 10, 342-355, ISSN Online: 2165-3860, ISSN Print: 2165-3852
19. Kamalesh Kumar Pandit, SinamIboton Singh, Dipak Sarma, ‘Heat and Mass Transfer Analysis of an Unsteady MHD Flow Past an Impulsively Started Vertical Plate in Presence of Thermal Radiation’International Journal of Fluid Mechanics & Thermal Sciences 2018; 4(2): 18-26ISSN: 2469-8105 (Print); ISSN: 2469-8113 (Online).
20. A. Khan and R. Solankiinitial‘Unsteady Free Convective Flow Past An Infinite Vertical Plate With Radiation And Mass Transfer’Effectsint. J. Of Applied Mechanics And Engineering, 2017, Vol.22, No.4, Pp.931-943 Doi: 10.1515/Ijame-2017-0060.